

Evaluation of Heat Evolution of Pastes Containing High Volume of Ground River Sand and Ground Granulated Blast Furnace Slag

Punnaman NORRARAT, Weerachart TANGCHIRAPAT, Chai JATURAPITAKKUL *

Department of Civil Engineering, Faculty of Engineering, King Mongkut's University of Technology Thonburi, Bangkok 10140, Thailand

crossref <http://dx.doi.org/10.5755/j01.ms.23.1.13579>

Received 05 November 2015; accepted 31 January 2016

This paper investigated the heat evolution of pastes containing inert and active materials with different particle sizes. Ground river sand was used as an inert material while ground granulated blast furnace (GGBF) slag was used as an active material. Ground river sand (GRS) and GGBF slag were ground to have the same particle size and were used separately as a replacement of Portland cement type I at rates of 50–70 % by weight of the binder. Heat evolution of pastes containing GRS and GGBF slag was measured using an isothermal conduction calorimeter up to 72 h. The results showed that GRS with different particle sizes had a slight effect on the heat evolution of pastes. GGBF slag with median particle size d_{50} of 4.4 μm and d_{50} of 17.8 μm had a small effect on the heat evolution of pastes during the first 24 h, and the pastes also had very low heat evolution for up to 72 h. At the same replacement rate of Portland cement, however, the heat evolution due to the slag reaction was slightly increased when the particle size of the GGBF slag was decreased. Finally, the higher is the cement replacement by GGBF slag, the higher is the slag reaction.

Keywords: heat evolution, inert material, active material, river sand, particle size, slag reaction.

1. INTRODUCTION

Blast furnace slag (BFS) is a by-product of the production of pig iron and consists of silicates and aluminosilicates of calcium. BFS exhibits hydraulic cementing properties when it is finely ground, and it is called ground granulated blast furnace (GGBF) slag when it is in that state [1]. GGBF slag has been used as a supplementary cementitious material (SCM) in blended cement for more than a century [2]. Annual worldwide production of GGBF slag has been estimated at 250 million tons per year [3]. The benefits of GGBF slag as a partial replacement of cement in concrete production include the enhancement of long-term strength and durability [4–6]. In addition, the cost of the concrete is reduced, and environmental problems due to the reduction of Portland cement production are mitigated [7, 8].

Hydration of ordinary Portland cement (OPC) and the GGBF slag reaction are chemical reactions between Portland cement, GGBF slag, and water. It is very complex and is an exothermic process. The major products of hydration are calcium silicate hydrate (C-S-H), calcium aluminate hydrate, and calcium hydroxide. The glass contents or amorphous phase from GGBF slag can be dissolved by hydroxyl ions liberated during the cement hydration; thereafter, GGBF slag can also react with sodium and potassium alkalis and calcium hydroxide to create additional C-S-H. In addition, the CaO in GGBF slag can create C-S-H from a hydration reaction similar to OPC but at a very slow rate [9]. The heat evolution of Portland cement pastes containing pozzolanic material or GGBF slag was measured using an isothermal conduction calorimeter at constant temperature in order to study the early hydration [10, 11].

Gruyaert et al. studied the hydration heat of pastes containing GGBF slag and found that the hydration heat contributed from the dilution effect, homogeneous nucleation, and gypsum content, at various cement replacement levels ranging from 30 % to 85 % [12]. Douglas et al. and Bougara et al. studied the reactivity of GGBF slag with different sizes and sources using an isothermal conduction calorimeter. They found that the partial replacement of Portland cement with GGBF slag reduces the heat evolution during the first 72 h [13, 14]. Han et al. and Ma et al. found that temperature affects the heat evolution specifically that the heat evolution of GGBF slag increases with the increase of the temperature [15, 16]. However, their study did not specify how much of the heat evolution of paste containing GGBF slag is contributed from cement hydration and from slag reaction.

The heat evolution during the hydration process is an important factor to consider for mass concretes, hot and cold weather concreting, and determining the reactivity. If the temperature difference within the mass concrete is too high, the concrete tends to crack due to differential expansion caused by different temperatures in the concrete that leads to a reduction in the durability of the concrete [17]. Gajda and Geem recommended that the allowable temperature difference between the core and the surface of a mass concrete structure should not exceed 19 °C [18]. To reduce the temperature effect, the replacement of Portland cement with an optimal dosage of pozzolan, such as fly ash and GGBF slag, can reduce the proportion of cement used in the concrete mix proportion and, thus, reduce the heat evolution, resulting in decreased thermal cracking during the early age of concrete structures [19].

* Corresponding author. Tel: +66-2-470-9314; fax: +66-2-427-9063.
E-mail address: chaijatura58@gmail.com (C. Jaturapitakkul)

The aim of this paper is to investigate the heat evolution of pastes containing non-reactive crystalline material (ground river sand) and GGBF slag.

The heat evolution contributed from cement hydration and slag reaction is analyzed and presented. Heat evolution produced by chemical reaction or physical changes as a function of time is measured using an isothermal conduction calorimeter at a constant temperature. The results will lead to a greater understanding of the heat evolution, cement hydration, and slag reaction of GGBF slag with different particle sizes. The findings would benefit users who apply GGBF slag in high volume for use in mass concrete.

2. MATERIAL AND METHODS

2.1. Materials

The main materials used in this study consisted of Portland cement type I (OPC), ground local river sand (GRS), and ground granulated blast furnace (GGBF) slag. GGBF slag is a by-product of the production of pig iron from Rayong Province, Thailand. OPC was used as a cementitious material while GRS was used as a non-reactive crystalline material.

To investigate the heat evolution and slag reaction, a non-reactive crystalline material (ground local river sand or GRS) was prepared and used in this study. To obtain GRS, local river sand was washed to get rid of impurities and carefully ground until the median particle sizes were the same as those of GGBF slag.

For large particle size: GRS and GGBF slag were separately and carefully ground to have the same median particle size (d_{50}) of $18 \pm 1 \mu\text{m}$. This size is specified as L (large-sized). It is noted that the L size of GRS and GGBF slag are almost the same size as that of OPC, which has d_{50} of $18.1 \mu\text{m}$. The intention of this process is to avoid the packing effect due to different particle sizes because GRS and GGBF slag have the same particle size as that of OPC.

For small particle size: GRS and GGBF slag were separately ground to have a median particle size of $5 \pm 1 \mu\text{m}$. This size is specified as S (small-sized) and is smaller than that of OPC. The intention of this process is to use SGRS and SGGBF slag that have a smaller particle size than OPC to investigate the heat evolution of pastes due to the packing effect of the small particle size.

OPC, GRS, and GGBF slag were measured for their d_{50} and particle size distributions by Sympatec's laser diffraction particle size analyzer (HELOS/H2399 & RODOS), and the procedure was in accordance with ISO 13320 [20]. Fig. 1 shows the comparison of the particle size distributions of OPC, GRS, and GGBF slag. It should be noted that the particle size distributions of OPC, LGRS, and LGGBF slag are nearly the same, and the median particle size, d_{50} , of the materials are in the range of $18 \pm 1 \mu\text{m}$, whereas SGRS and SGGBF slag have slightly different in particle size distributions and the d_{50} of both materials are in the range of $5 \pm 1 \mu\text{m}$.

2.2. Physical properties of the materials

Physical properties of OPC, GRS, and GGBF slag with different particle sizes are given in Table 1. Specific gravity

and the particle retained on a sieve No. 325 of the materials were determined in accordance with ASTM C 188 [21] and C 430 [22], respectively. The median particle size (d_{50}) of OPC is $18.1 \mu\text{m}$, while those for LGRS and SGRS are 17.7 and $4.8 \mu\text{m}$, respectively. LGGBF and SGGBF slag have median particle sizes, d_{50} , of 17.8 and $4.4 \mu\text{m}$, respectively.

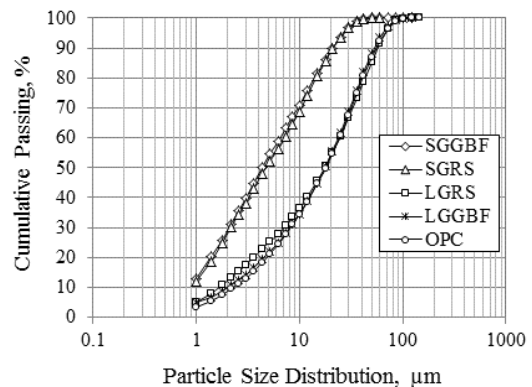


Fig. 1. Particle size distributions of the materials

Table 1. Physical properties of OPC, GRS, and GGBF slag

Material	Specific gravity	Retained on a No.325 sieve, %	Median particle size, μm
OPC	3.15	16.6	18.1
LGRS	2.61	17.9	17.7
SGRS	2.63	1.1	4.8
LGGBF	2.92	12.2	17.8
SGGBF	2.92	2.4	4.4

The mineralogical compositions of GRS and GGBF slag were determined by quantitative X-ray diffraction analysis, as shown in Table 2. LGRS and SGRS have 100 % crystalline phases such as quartz, microcline, albite, and muscovite whereas LGGBF and SGGBF slag have 99.2 and 99.6 % amorphous or glass content. Because LGRS and SGRS have 100 % crystalline phases, they cannot react with OPC or GGBF slag to form any hydration products. Fig. 2 shows the X-ray diffraction patterns of SGGBF slag and SGRS, respectively. The figures also show that SGRS is mostly in a crystalline phase, whereas SGGBF slag is in an amorphous phase. The particle shapes of OPC, LGRS, and LGGBF slag are shown in Fig. 3, and all of them are solid with angular particle shapes.

2.3. Chemical compositions of materials

Chemical compositions of OPC, SGRS, and SGGBF slag, which were determined using X-ray fluorescence, are shown in Table 3. The main chemical components of OPC are 65.0 % CaO, 19.5 % SiO₂, 5.3 % Al₂O₃, and 3.2 % Fe₂O₃, whereas the chemical components of SGRS are 92.0 % SiO₂ and 5.0 % Al₂O₃. The SiO₂ of SGRS is in the form of quartz, thus, it is not a pozzolanic material. Similar results were reported for ground river sand, which contains approximately 91.8–92.9 % SiO₂ (quartz) [23–25]. The chemical components of SGGBF slag are 35.3 % CaO, 36.0 % SiO₂, 14.6 % Al₂O₃, and 7.1 % MgO. Other minor components include alkali oxides and iron oxides.

Table 2. Mineralogical compositions of GRS and GGBF slag

Name	Crystalline, %				Amorphous, %	Total crystalline, %	Total amorphous, %
	Quartz	Microcline	Albite	Muscovite			
LGRS	79.4	13.6	3.9	3.1	–	100	0
SGRS	79.4	13.8	3.8	3.0	–	100	0
LGGBF	0.8	–	–	–	99.2	0	100
SGGBF	0.4	–	–	–	99.6	0	100

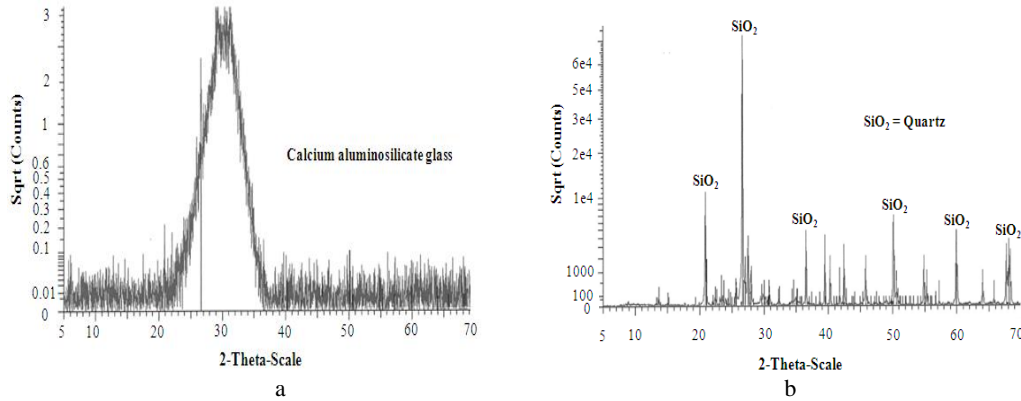


Fig. 2. X-ray diffraction patterns of materials: a – SGGBF slag; b – SGRS

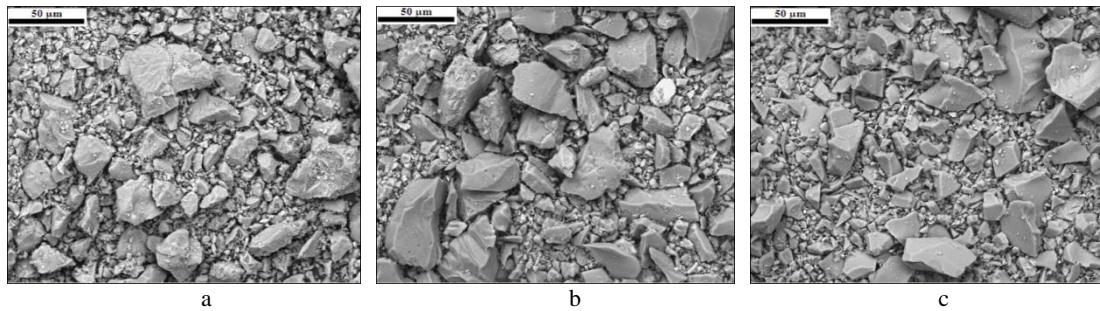


Fig. 3. Particle shapes of materials by SEM: a – OPC; b – LGRS; c – LGGBF

Table 3. Chemical compositions of OPC, SGRS, and SGGBF

Name	Chemical composition, %								
	SiO ₂	Al ₂ O ₃	Fe ₂ O ₃	CaO	MgO	SO ₃	Na ₂ O ₃	K ₂ O	LOI
OPC	19.5	5.3	3.2	65.0	0.8	2.7	0.1	0.4	2.4
SGRS	92.0	5.0	0.6	0.2	0.1	0.0	0.4	0.8	0.1
SGGBF	36.0	14.6	1.9	35.3	7.1	2.0	0.9	0.2	0.1

2.4. Heat evolution of paste

To evaluate the heat evolution, three types of pastes, control paste made with OPC (control paste), non-reactive crystalline material pastes (GRS pastes), and GGBF slag pastes, were prepared and investigated in this study. Two particle sizes of GRS (LGRS and SGRS) and GGBF slag (LGGBF and SGGBF slag) were used separately to replace OPC at rates of 0, 50, 60, and 70 % by weight of the binder (OPC + GRS or OPC + GGBF slag) to cast pastes. The water to binder (W/B) ratio of all pastes was kept constant at 0.50. The mix proportions of OPC paste and pastes containing GRS and GGBF slag are shown in Table 4.

To measure the heat evolution of the pastes, a thermal activity monitor (the TAM Air calorimeter from TA Instruments, No. 387, USA) was used, and the procedure was in accordance with ASTM C 1702 [26]. The TAM Air calorimeter is shown in Fig. 4. The TAM Air contains 8 parallel twin calorimeters (sample and reference) as the type of measurement channels. The binders are prepared and then placed in two glass ampoules at a controlled temperature of

25 °C and inserted in the TAM Air calorimeter with the same temperature.

Table 4. Mix proportions of pastes by weight

Mixture	OPC	GRS	GGBF	W/B
Control	1	–	–	0.5
LGRS50	0.5	0.5	–	0.5
LGRS60	0.4	0.6	–	0.5
LGRS70	0.3	0.7	–	0.5
SGRS50	0.5	0.5	–	0.5
SGRS60	0.4	0.6	–	0.5
SGRS70	0.3	0.7	–	0.5
LGGBF50	0.5	–	0.5	0.5
LGGBF60	0.4	–	0.6	0.5
LGGBF70	0.3	–	0.7	0.5
SGGBF50	0.5	–	0.5	0.5
SGGBF60	0.4	–	0.6	0.5
SGGBF70	0.3	–	0.7	0.5

The binders were OPC (or OPC+GRS, or OPC+GGBF slag), and the reference was quartz (Ottawa sand). For the mixing procedure, the combinations of OPC, OPC+GRS or

OPC+GGBF slag and deionized water were mixed together by using plastic paddle until the uniformity of all pastes was obtained.

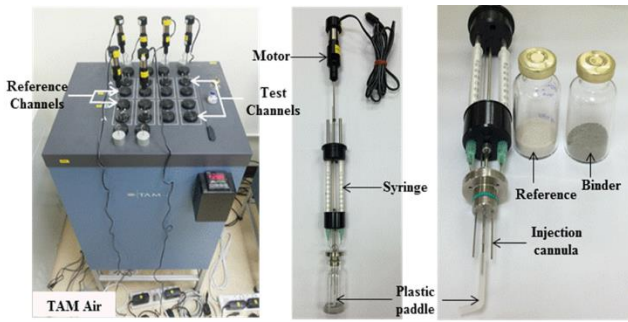


Fig. 4. Thermal activity monitor (TAM)

The signal heat flow was controlled using a computer program, and output data on the cumulative heat evolution versus time were recorded. The heat evolution was measured until the end of the testing period, which was 72 h after mixing.

3. RESULTS AND DISCUSSION

3.1. Effect of GRS particles on the cumulative heat evolution

Fig. 5 shows the relationship between the cumulative heat evolution and time of the OPC paste and pastes containing GRS at the cement replacement rates of 50, 60, and 70 % by weight of the binder, respectively.

The results indicated that the pastes, when mixed with a small particle size of SGRS ($d_{50} = 4.8 \mu\text{m}$) and large particle size of LGRS ($d_{50} = 17.7 \mu\text{m}$), provided a much lower cumulative heat evolution than that of the OPC paste. A similar trend was also reported by Douglas et al. who replaced Portland cement with 35 and 50 % sand in the mixtures and found that the cumulative heat evolution of those pastes was the lowest compared to the OPC paste and GGBF slag paste [13].

Fig. 6 shows the cumulative heat evolution and the replacement of cement by GRS with different particle sizes at 24 and 72 h. It revealed that the cumulative heat evolution of SGRS and LGRS pastes with the same replacement and same age were very similar. The cumulative heat evolution of LGRS paste was a little lower than that of SGRS paste at the same replacement percentage and same age. For example, the LGRS70 and SGRS70 pastes had a cumulative heat evolution of 79.1 and 83.9 J/g at 24 h, respectively, and it increased to 120.9 and 128.0 J/g at 72 h, respectively, while the OPC paste had a cumulative of heat evolution of 213.7 J/g at 24 h, and it increased to 311.8 J/g at 72 h. SGRS70 paste produced a higher cumulative heat evolution than that of LGRS50 paste because the small particle size of SGRS produced a packing effect, creating a more homogeneous paste, and accelerated the hydration reaction of OPC [27].

However, it was noticed that the different particle sizes of GRS (d_{50} of 4.8 μm and 17.7 μm) had a small effect on the cumulative heat evolution because GRS is a non-reactive material (SiO_2 of GRS is in the form of quartz); thus, it is not a pozzolanic material and cannot react with Portland cement to create heat due to the chemical reaction [28].

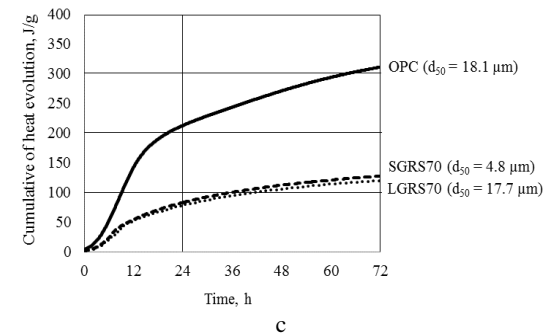
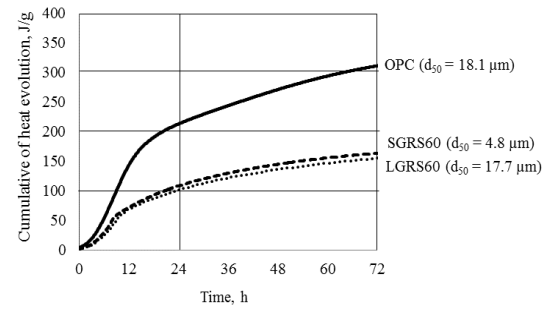
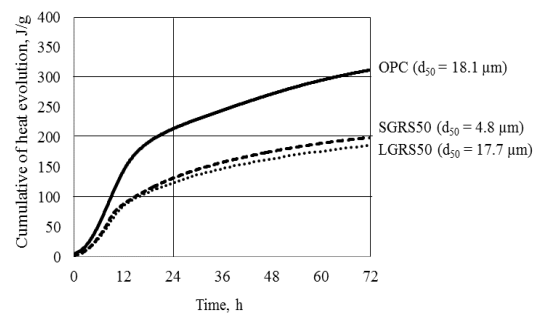


Fig. 5. Cumulative heat evolution of GRS pastes with different particle sizes: a–50 % replacement of Portland cement; b–60 % replacement of Portland cement; c–70 % replacement of Portland cement

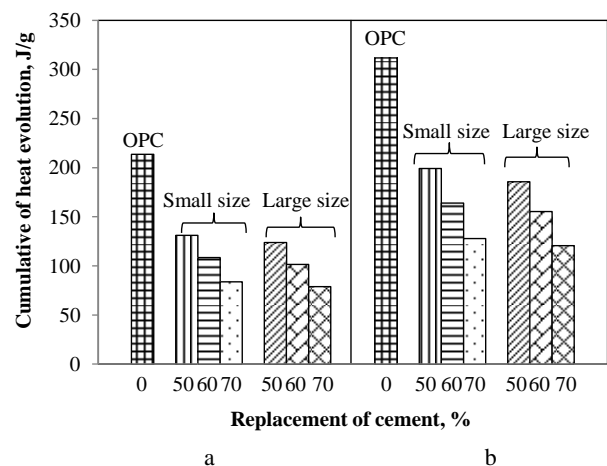


Fig. 6. Cumulative heat evolution of GRS pastes: a–24 h; b–72 h

Because OPC and LGRS have almost the same particle size distributions (both materials have d_{50} of $18 \pm 1 \mu\text{m}$), the cumulative heat evolution of LGRS50, LGRS60, and LGRS70 pastes (OPC contents of 50, 40, and 30 % by weight of the binder) was assumed to be only from cement hydration. The cumulative heat evolution of LGRS pastes due to cement hydration is shown in Table 5. At the same

ages (12, 24, 36, 48, 60, or 72 h), the cumulative heat evolution due to cement hydration of GRS pastes decreased with the increase of GRS replacement.

Table 5. Cumulative heat evolution of pastes

Name	Cumulative of heat evolution, J/g					
	12h	24h	36h	48h	60h	72h
OPC	143.9	213.7	244.5	271.8	294.6	311.8
LGRS50	85.1	123.8	147.3	163.7	176.3	185.9
LGRS60	69.2	101.6	122.4	136.6	147.4	155.6
LGRS70	52.9	79.1	95.3	106.5	114.7	120.9
SGRS50	87.8	131.3	157.6	175.8	189.4	199.2
SGRS60	72.6	108.8	130.4	145.5	156.4	164.1
SGRS70	55.3	83.9	101.0	113.0	121.5	128.0
LGGBF50	79.2	115.8	140.5	158.7	173.6	186.6
LGGBF60	62.1	95.4	118.0	135.8	150.4	162.8
LGGBF70	46.8	72.8	92.7	109.4	124.0	136.9
SGGBF50	76.2	120.9	152.3	178.0	199.8	218.5
SGGBF60	62.0	99.0	128.5	153.8	175.8	195.2
SGGBF70	45.5	75.1	101.5	127.3	150.7	170.7

For example, the cumulative heat evolution of OPC paste was 213.7 J/g at 24 h, and it increased to 311.8 J/g at 72 h, while those of the LGRS50, LGRS60, and LGRS70 pastes were 123.8, 101.6, and 79.1 J/g (approximately 57.9, 47.5, and 37.0 % of OPC paste) at 24 h and then slightly increased to 185.9, 155.6, and 120.9 J/g (approximately 59.6, 49.9, and 38.8 % of OPC paste) at 72 h.

3.2. Effect of GGBF slag particles on the cumulative heat evolution

The cumulative heat evolution of pastes containing GGBF slag at cement replacement rates of 50, 60, and 70 % by weight of the binder compared to Portland cement paste (OPC paste) is shown in Fig. 7. It was found that the OPC paste ($d_{50} = 18.1 \mu\text{m}$) had the highest cumulative heat evolution of 213.7 J/g at 24 h, and it increased to 311.8 J/g at 72 h. This result was close to the result obtained by Bougara et al. who found that the cumulative heat evolution of OPC was 290 J/g at 72 h [14].

Fig. 7 show that the cumulative heat evolution of OPC, SGGBF, and LGGBF pastes increased very quickly up to 12 h and increased constantly afterwards. In addition, the cumulative heat evolution of pastes containing GGBF slag decreased with the increase of GGBF slag replacement. This is due to the reduction of Portland cement which has higher heat evolution than GGBF slag. The cumulative heat evolution of pastes mixed with SGGBF ($d_{50} = 4.4 \mu\text{m}$) and LGGBF ($d_{50} = 17.8 \mu\text{m}$) was much lower than that of the OPC ($d_{50} = 18.1 \mu\text{m}$) paste at the same age. For example, the SGGBF70 and LGGBF70 pastes had a cumulative heat evolution of 170.7 J/g and 136.9 J/g, i.e., only 54.7 and 43.9 % of OPC paste, at 72 h, respectively. This confirmed that the use of GGBF slag to replace OPC can reduce the heat evolution of concrete which is an important factor to be considered in mass concrete structures. This result is also consistent with the previous research [12–14] that concluded that GGBF slag can be used to reduce the heat evolution of concrete.

The cumulative heat evolution and the replacement of cement by GGBF slag with different particle sizes at 24 and 72 h is illustrated in Fig. 8. The figures show that the

cumulative heat evolution of the small particle size and large particle sizes of GGBF pastes are slightly different at 24 h.

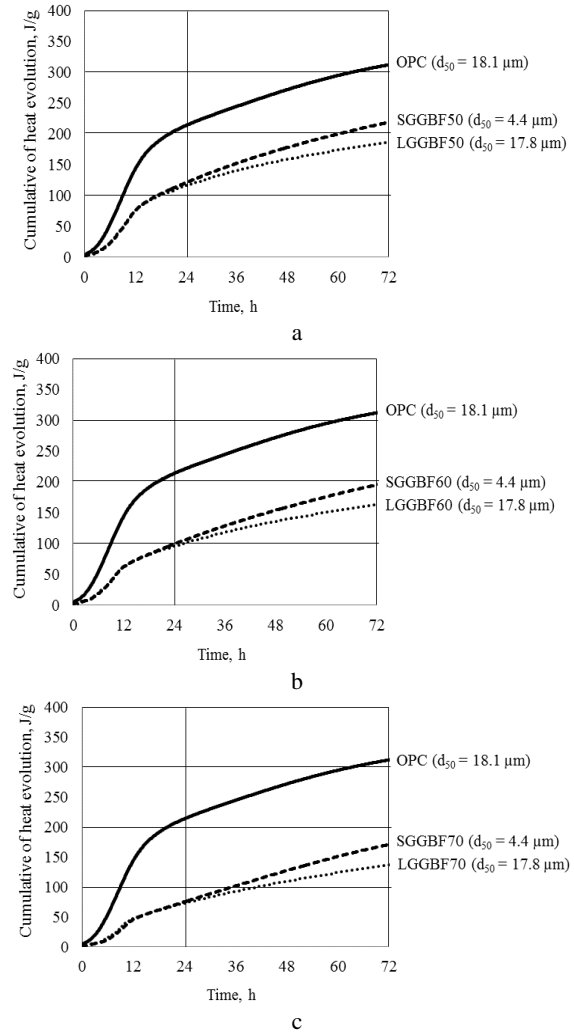


Fig. 7. Cumulative heat evolution of GGBF pastes with different particle sizes: a–50 % replacement of OPC; b–60% replacement of OPC; c–70% replacement of OPC

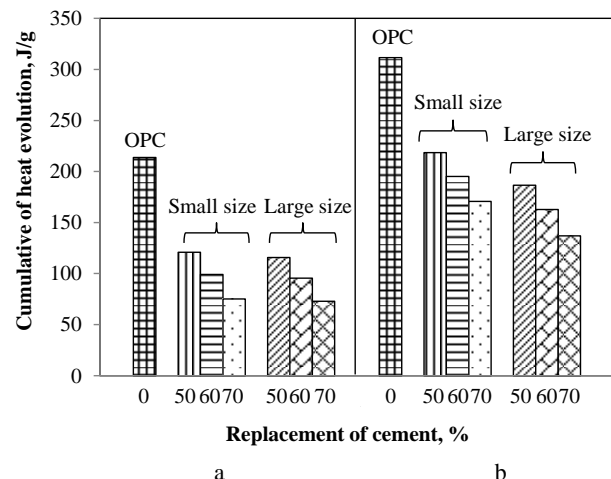


Fig. 8. Cumulative heat evolution of GGBF slag pastes: a–24 h; b–72 h

However, the pastes with the smaller size of GGBF slag tend to produce a higher cumulative heat evolution than does the larger size at 72 h. Similar results were also reported by Zhang, et al. who found that the heat evolution

of paste containing GGBF slag increased with the increased of GGBF slag fineness [10]. For example, LGGBF50 paste had a cumulative heat evolution of 115.8 J/g at 24 h, and it increased to 186.6 J/g at 72 h, while SGGBF50 paste had a cumulative heat evolution of 120.9 J/g at 24 h, and it increased to 218.5 J/g at 72 h. This is due to the smaller size of SGGBF slag having a higher surface area than LGGBF slag, thus increasing the slag activity and acting as nucleation sites [29, 30] to promote the cement hydration and slag reaction.

3.3. Cumulative heat evolution due to the slag reaction

One objective of this study is to determine the value of the cumulative heat evolution due to the slag reaction. To obtain this, the cumulative heat evolution of paste due to the packing effect of the small particles has to be considered and taken out from the total cumulative heat evolution. Thus, the difference in the cumulative heat evolution between GGBF slag paste and GRS paste at the same particle size, same replacement, same W/B ratio, and same age is the cumulative heat evolution due to the slag reaction of GGBF slag. For example, the cumulative heat evolution due to the slag reaction of SGGBF70 paste at 72 h can be calculated by using the cumulative heat evolution of paste SGGBF70 (170.7 J/g) in Table 5 minus the cumulative heat evolution of SGRS50 paste (128.0 J/g) in Table 5, which is equal to 42.7 J/g in Table 6.

Table 6. Values of cumulative heat evolution of pastes due to the slag reaction

Compared paste	Size of material particles, μm	Cumulative of heat evolution due to slag reaction, J/g					
		12h	24h	36h	48h	60h	72h
LGGBF50-LGRS50	18 \pm 1	-5.9	-8.0	-6.7	-5.0	-2.7	0.8
LGGBF60-LGRS60		-7.1	-6.3	-4.4	-0.8	2.9	7.3
LGGBF70-LGRS70		-6.1	-6.2	-2.7	3.0	9.3	16.0
SGGBF50-SGRS50	5 \pm 1	-11.7	-10.4	-5.4	2.2	10.4	19.3
SGGBF60-SGRS60		-10.6	-9.9	-1.9	8.3	19.3	31.1
SGGBF70-SGRS70		-9.8	-8.8	0.5	14.3	29.2	42.7

Table 6 shows the values of the cumulative heat evolution of pastes due to the slag reaction. The differences in cumulative heat evolution for the pastes LGGBF50 and LGRS50 (LGGBF50-LGRS50) at 12, 24, 36, 48, 60, and 72 h were -5.9, -8.0, -6.7, -5.0, -2.7, and 0.8 J/g, respectively, while those for the pastes SGGBF50-SGRS50 were -11.7, -10.4, -5.4, 2.2, 10.4, and 19.3 J/g, respectively. The minus sign indicates that the use of GGBF slag (LGGBF or SGGBF paste) in the paste resulted in a lower cumulative heat evolution compared to GRS paste (LGRS or SGRS). This suggests that, when Portland cement type I was replaced by GGBF slag, regardless of its particle size (smaller or larger, up to a d_{50} of 18 μm), there was no apparent cumulative heat evolution due to the slag reaction during the first 24 h. This result also indicates that the GGBF slag retards the cement hydration at an early age.

At 72 h, the values of the cumulative heat evolution due to the slag reaction of the LGGBF50, LGGBF60, and LGGBF70 pastes were 0.8, 7.3, and 16.0 J/g, respectively

whereas those of the SGGBF50, SGGBF60, and SGGBF70 pastes were 19.3, 31.1, and 42.7 J/g, respectively. This finding suggests that the cumulative heat evolution due to the slag reaction increases with the decrease of particle size and cement replacement by GGBF slag. The results also indicate that SGGBF and LGGBF slags have slow reaction at early age, which is due to low hydraulic activity and leads to the low early compressive strength as generally found when GGBF slag is used to replace OPC in concrete [31–33].

It should be noted that paste containing GGBF slag with the highest cumulative heat evolution did not necessarily have the highest slag reaction. For example, the cumulative heat evolution of the pastes SGGBF50 and SGGBF70 during the first 72 h was 218.5 and 170.7 J/g while their cumulative heat evolution due to the slag reaction was 19.3 and 42.7 J/g, respectively. This suggests that, for the same particle size of GGBF slag, the cumulative heat evolution due to the slag reaction depended on the dosage of cement replacement by the GGBF slag.

4. CONCLUSIONS

When using ground river sand with the median particle sizes (d_{50}) of 4.8 and 17.7 μm to replace Portland cement type I at the same replacement of 50–70 % by weight of the binder, the cumulative heat evolution of both pastes are nearly the same during the first 72 h.

The cumulative heat evolution due to the slag reaction increased with the decrease of GGBF slag particles. Moreover, the cumulative heat evolution at 72 h of GGBF slag was much lower than that of Portland cement.

At 24 h, the use of GGBF slag to replace Portland cement type I at 50–70 % by weight of the binder could reduce the cumulative heat evolution because GGBF slag acted like a retarder and the values of the cumulative heat evolution of pastes containing GGBF slag at 72 h were low.

When GGBF slag with d_{50} of 4.4 μm was used to replace OPC at 50, 60, and 70 % by weight of the binder, the cumulative heat evolution of GGBF slag pastes at 24 h were 56.6, 46.3, and 35.1 % that of OPC paste and increased to 70.1, 62.6, and 54.7 % that of OPC paste at 72 h, respectively. In addition, the use of GGBF slag with d_{50} of 17.8 μm to replace OPC at 50, 60, and 70 % by weight of the binder had the cumulative heat evolution of 54.2, 44.6, and 33.8 % that of OPC paste at 24 h, and it increased to 59.9, 52.2, and 43.9 % that of OPC paste at 72 h.

The use of GGBF slag with d_{50} of 17.8 μm to replace OPC at 50, 60, and 70 % by weight of the binder produced a cumulative heat evolution at 72 h due to the slag reaction of 0.8, 7.3, and 16.0 J/g, respectively, while the use of GGBF slag with d_{50} of 4.4 μm had a cumulative heat evolution due to the slag reaction at 72 h of 19.3, 31.1, and 42.7 J/g, respectively.

Acknowledgments

The authors gratefully acknowledge the financial support from the Office of the Higher Education Commission under National Research University (NRU) at King Mongkut's University of Technology Thonburi. Thanks are also extended to the Siam Research and

Innovation Co., Ltd for providing facilities and equipment for this study.

REFERENCES

1. **ACI 233R-03.** Slag Cement in Concrete and Mortar *ACI Manual of Concrete Practice* 2012: pp. 1–19.
2. **Bellmann, F., Stark, J.** Activation of Blast Furnace Slag by a New Method *Cement and Concrete Research* 39 (8) 2009: pp. 644–650.
3. **Boukendakdji, O., Kadri, E.H., Kenai, S.** Effects of Ground Granulated Blast Furnace Slag and Superplasticizer Type on the Fresh Properties and Compressive Strength of Self-Compacting *Concrete Cement and Concrete Composites* 34 (4) 2012: pp. 583–590.
<https://doi.org/10.1016/j.cemconcomp.2011.08.013>
4. **Sivasundaram, V., Malhotra, V.M.** Properties of Concrete Incorporating Low Quality of Cement and High Volumes of Ground Granulated Slag *ACI Materials Journal* 89 (6) 1992: pp. 554–563.
5. **Guneyisi, E., Gesoglu, M.** A Study on Durability Properties of High Performance Concretes Incorporating High Replacements of Slag *Materials and Structures* 41 2008: pp. 479–493.
6. **Bouikni, A., Swamy, R.N., Bali, A.** Durability Properties of Concrete Containing 50% and 65% Slag *Construction and Building Materials* 23 (8) 2009: pp. 2836–2845.
<https://doi.org/10.1016/j.conbuildmat.2009.02.040>
7. **Metha, P.K.** Reducing the Environmental Impact of Concrete *Concrete International* 23 (10) 2001: pp. 61–66.
8. **Kurt, M., Gul, M.S., Gul, R., Aydin, A.C., Kotan, T.** The Effect of Pumice Powder on the Self-Compactability of Pumice Aggregate Lightweight Concrete *Construction and Building Materials* 103 2016: pp. 36–46.
9. **Shi, C., Day, R.L.** A Calorimetric Study of Early Hydration of Alkali-Slag Cement *Cement and Concrete Research* 25 (6) 1995: pp. 1333–1346.
[https://doi.org/10.1016/0008-8846\(95\)00126-W](https://doi.org/10.1016/0008-8846(95)00126-W)
10. **Zhang, T., Yu, Q., Wei, J., Gao, P., Zhang, P.** Study on Optimization of Hydration Process of Blended Cement *Journal Thermal Analysis and Calorimetry* 107 2012: pp. 489–498.
<https://doi.org/10.1007/s10973-011-1531-8>
11. **Siler, P., Kratky, J., De Belie, N.** Isothermal and Solution Calorimetry to Assess the Effect of Superplasticizers and Mineral Admixtures on Cement Hydration *Journal Thermal Analysis and Calorimetry* 107 2012: pp. 313–320.
12. **Gruyaert, E., Robeyst, N., De Belie, N.** Study of Hydration of Portland Cement Blended with Blast Furnace Slag by Calorimetry and Thermogravimetry *Journal Thermal Analysis and Calorimetry* 102 2010: pp. 941–951.
13. **Douglas, E., Elola, A., Malhotra, V.M.** Characterization of Ground Granulated Blast Furnace Slag and Fly Ashes and their Hydration in Portland Cement Blends *Cement and Concrete Aggregates* 12 (2) 1990: pp. 38–46.
14. **Bougara, A., Lynsdale, C., Milestone, N.B.** Reactivity and Performance of Blast Furnace Slags of Differing Origin *Cement and Concrete Composites* 32 (4) 2010: pp. 319–324.
15. **Han, F., Zhang, Z., Wang, D., Yan, P.** Hydration Kinetics of Composite Binder Containing Slag at Different Temperatures *Journal Thermal Analysis and Calorimetry* 121 (2) 2015: pp. 815–827.
16. **Ma, W., Sample, D., Martin, R., Brown, P.W.** Calorimetric Study of Cement Blends Containing Fly Ash, Silica Fume, and Sag at Elevated Temperatures *Cement and Concrete Aggregates* 16 (2) 1994: pp. 93–99.
17. **ACI 207.1R-05.** Guide to Mass Concrete *ACI Manual of Concrete Practice* 2012: pp. 1–30.
18. **Gajda, J., Geem, M.V.** Controlling Temperatures in Mass Concrete *Concrete International* 24 (1) 2002: pp. 59–62.
19. **Metha, P.K.** Durability: Critical Issues for the Future *Concrete International* 19 (7) 1997: pp. 27–33.
20. ISO 13320-09. Particle Size Analysis-Lazer Diffraction Methods, International Standard, 2009: pp. 1–56.
21. ASTM C 188: Standard Test Method for Density of Hydraulic Cement, 2014.
22. ASTM C 430: Standard Test Method for Fineness of Hydraulic Cement by the 45- μm (No.325) Sieve, 2014.
23. **Jaturapitakkul, C., Tangpagasit, J., Songmue, S., Kiattikomol, K.** Filler Effect and Pozzolanic Reaction of Ground Palm Oil Fuel Ash *Construction and Building Materials* 25 (11) 2011: pp. 4287–4293.
24. **Tangpagasit, J., Cheerarot, R., Jaturapitakkul, C., Kiattikomol, K.** Packing Effect and Pozzolanic Reaction of Fly Ash in Mortar *Cement and Concrete Research* 35 (6) 2005: pp. 1145–1151.
25. **Yang, Q., Zhang, S., Huang, S., He, Y.** Effect of Ground Quartz Sand on Properties of High Strength Concrete in the Steam Autoclaved Curing *Cement and Concrete Research* 30 (12) 2000: pp. 1993–1998.
26. ASTM C 1702: Standard Test Method for Measurement of Heat of Hydration of Hydraulic Cementitious Materials using Isothermal Conduction Calorimetry, 2014.
27. **Sinsiri, T., Chindaprasirt, P., Jaturapitakkul, C.** Influence of Fly Ash Fineness and Shape on the Porosity and Permeability of Blended Cement Pastes *International Journal of Mineral, Metal, metallurgy, and Matererials* 17 (6) 2010: pp. 683–690.
28. **Kiattikomol, K., Jaturapitakkul, C., Tangpagasit, J.** Effect of Insoluble Residue on Properties of Portland Cement *Cement and Concrete Research* 30 (8) 2000: pp. 1209–1214.
[https://doi.org/10.1016/S0008-8846\(00\)00315-X](https://doi.org/10.1016/S0008-8846(00)00315-X)
29. **Moosberg-Bustnes, H., Lagerblad, B., Forssberg, E.** The Function of Fillers in Concrete *Materials and Structures* 37 (2) 2004: pp. 74–81.
30. **De Weerd, K., Ben Hara, M., Le Saout, G., Kjellsen, K.O., Justnes, H., Lothenbach, B.** Hydration Mechanisms of Ternary Portland Cements Containing Limestone Powder and Fly Ash *Cement and Concrete Research* 41 (3) 2011: pp. 279–291.
31. **Bougara, A., Lynsdale, L., Ezziane, K.** Activation of Algerian slag in mortars *Construction Building Material* 23 (1) 2009: pp. 542–547.
32. **Shariq, M., Prasad, J., Masood, A.** Effect of GGBFS on Time Dependent Compressive Strength of Concrete *Construction and Building Materials* 24 (8) 2010: pp. 1469–1478.
33. **Daequennes, A., Espion, B., Staquet, S.** How to Assess the Hydration of Slag Cement Concrete *Construction and Building Materials* 40 2013: pp. 1012–1020.